Photo-induced spin auto-oscillations and autowaves in magnets

1997 J. Phys.: Condens. Matter 9 5655

(http://iopscience.iop.org/0953-8984/9/26/013)

J. Phys.: Condens. Matter **9** (1997) 5655–5670. Printed in the UK PII: S0953-8984(97)78074-3

Photo-induced spin auto-oscillations and autowaves in magnets

S N Lyakhimets†, B A Ivanov and A A Zhmudsky
NASU Institute of Magnetism, 36 (b) Vernadskii av, 252142, Kiev, Ukraine

Received 25 September 1996

Abstract. The theory of light-induced formation of spin autowaves in weak ferromagnets, such as $FeBO_3$, caused by special non-equilibrium photo-induced magnetic anisotropy is constructed. The description is based on the coupled set of phenomenological equations for the iron sublattice magnetizations and for the parameters describing the induced anisotropy. The theoretical results are in good agreement with the experimental data. Some bifurcations of the solution appear with the changing of the parameters of the magnet.

1. Introduction

The investigation of self-sustaining space homogeneous and inhomogeneous oscillation (auto-oscillations and autowaves) is of great importance in non-equilibrium physics of condensed matter. Such effects were found in low-temperature physics of magnetic materials by Fedorov and his collaborators [1]. In these and further [2, 3] investigations, the dynamic state, caused by the unpolarized non-coherent optical radiation, in a thin plate of iron borate ($FeBO_3$) with nickel impurities ($FeBO_3$:Ni) was observed. The state appears to be a periodic structure (with a period of $\Lambda \sim 100$ mm) of magnetization inhomogeneity spreading in a crystal with velocity V of the order of 10 μm s^{-1}. It may be interpreted as a low-frequency magnetization autowave; its frequency ($\omega = 2\pi V/\Lambda \sim (10\text{–}10^2)$ s^{-1}) is several orders less than the velocity and the amplitude ($\leqslant 10^\circ$) considerably exceeds the usual nonlinear spin waves (for example, excited by the parallel pumping, see [4]) characteristics. The authors of [1] connected the appearance of these autowaves with unusual properties of photo-induced uniaxial magnetic anisotropy (PUMA) in $FeBO_3$:Ni.

Induced anisotropy is known to take place in some magnets, with the anisotropy axis direction depending on the magnetization direction in previous time moments [5]. Note that induced anisotropy can be observed in the absence of radiation (without external excitation), i.e. at the equilibrium state. At equilibrium and in some non-equilibrium cases, for example PUMA in $FeBO_3$ with copper and manganese impurities, the easy axis of the induced anisotropy is parallel to the magnetization. The induced anisotropy in this case stabilizes the instantaneous direction of magnetization which is well known for a number of magnetic materials [5].

However, for $FeBO_3$:Ni (also for $FeBO_3$:Cr and for pure iron borate) the situation is different: the easy axis of PUMA is perpendicular to the magnetization direction. This fact was shown in the experiments on domain-wall, shifting susceptibility [6] and the acoustic

† Deceased.

0953-8984/97/265655+16$19.50

resonance measurements [7]. Hence PUMA in $FeBO_3$:Ni destabilizes any magnetization distribution that generally may cause some auto-oscillations [1].

In [8] the equation that describes the magnetization dynamics, with PUMA being taken into account, was proposed and a small-amplitude autowave theory was proposed for materials such as $FeBO_3$:Ni. Similar equations were obtained later in [9] on the basis of microscopic consideration of $FeBO_3$ magnetization dynamics, taking into account the interaction with the degenerate magnetic impurity subsystem.

In [8] only weakly-nonlinear autowaves with small amplitude A, $A \ll 1$, were considered. We will show that, with reasonable assumptions about the relationship between the parameters describing PUMA and crystalline in-plane magnetic anisotropy, strongly nonlinear auto-oscillation regimes may take place in $FeBO_3$:Ni. The change of the system parameters causes a complicated set of bifurcation changes in a limit cycle that describes the auto-oscillations.

2. The model and the stability of the magnetic homogeneous state

The magnetization dynamics for a two-sublattice weak ferromagnet such as $FeBO_3$ can be described by the σ-model equation for a unit vector of antiferromagnetism $\boldsymbol{l}$. The magnetization $\boldsymbol{M}$ is determined by $\boldsymbol{l}$ and its time derivative (see for details the review articles [10]). The $FeBO_3$ in-plane anisotropy is considerably smaller than the uniaxial one and we may take into account only the in-plane dynamics of the vector $\boldsymbol{l}$ (in the easy plane xy only). In this case, $\boldsymbol{l}$ orientation is determined by one angle φ only. The following dynamic equation for φ can be written:

$$\alpha\left(\frac{1}{c^2}\frac{\partial^2\varphi}{\partial t^2} - \nabla^2\varphi\right) + F(\varphi) + \lambda\frac{\partial\varphi}{\partial t} = 0. \tag{1}$$

Here α is the inhomogeneous exchange constant, c is the spin wave velocity, λ is the relaxation constant and $F(\varphi)$ determines the magnetic anisotropy. For a rhombohedral magnet such as $FeBO_3$, the magnetization $\boldsymbol{m}$ can be expressed in the form

$$\boldsymbol{m} = m_{0\perp}(\boldsymbol{e}_x\cos\varphi + \boldsymbol{e}_y\sin\varphi) + [m_{0z}\sin 3\varphi + (2/g)(\partial\varphi/\partial t)]\boldsymbol{e}_z$$

where $m_{0\perp}$ and m_{0z} are determined by two independent invariants of the Dzyaloshinskii interaction, $m_{0z} \ll m_{0\perp}$, and g is the giromagnetic ratio, see [10]. The dynamic contribution to the magnetization for low-frequency autowaves $(\boldsymbol{m})_{dyn} \propto \partial\varphi/\partial t$ is small and may be omitted.

For the usual crystalline anisotropy $F(\varphi) = \partial w_a(\varphi)/\partial\varphi$, where $w_a(\varphi)$ is the anisotropy energy, i.e. $F = \beta_n \sin n\varphi$ ($n = 2,4,6$ for rhombic, tetragonal, rhombohedral and hexagonal magnets, respectively). The account of the magnetic field $\boldsymbol{H}$ in the basal plane leads to $F(\varphi) = h\sin\varphi$, where $h = Hm_{0\perp}/M_0^2$ and M_0 is the sublattice magnetization.

PUMA in $FeBO_3$ is determined by the orientation of the twofold anisotropy axis in the crystal basal plane. The corresponding contribution of F_{pi} to $F(\varphi)$ is characterized by parameters K_1 and K_2 and may be written as

$$F_{pi} = -2(K_1\cos 2\varphi - K_2\sin 2\varphi).$$

The values of K_1 and K_2 at the moment t depend on the shape of the $\varphi(t')$ function at $t' < t$. According to the commonly used theory of induced anisotropy [5], its time dependence is determined by the dissipation equation,

$$\tau\frac{\mathrm{d}K_1}{\mathrm{d}t} = \left(\frac{1}{2}f\sin 2\varphi - K_1\right) \qquad \tau\frac{\mathrm{d}K_2}{\mathrm{d}t} = \left(\frac{1}{2}f\cos 2\varphi - K_2\right) \tag{2}$$

where f is the constant characterizing the PUMA intensity and τ is the PUMA relaxation time. Further we shall be convinced that the case of $FeBO_3$:Ni corresponds to $f > 0$, i.e. with destabilization of a static distribution. The equation (1) for φ, along with (2); describes a self-consistent dynamics of the magnetic spin subsystem and PUMA-determining impurity subsystem. Let us introduce the angle ψ describing the PUMA axis direction according to the formula

$$K_1 = \kappa \sin 2\psi \qquad K_2 = \kappa \cos 2\psi.$$

Thus we shall write down the full set of equations as

$$\frac{\alpha}{c^2}\frac{\partial^2\varphi}{\partial t^2} - \alpha\nabla^2\varphi + \lambda\frac{\partial\varphi}{\partial t} + \beta_n \sin n\varphi = 2\kappa \sin\Phi \qquad \Phi = 2(\varphi - \Psi)$$
$$\tau\frac{\mathrm{d}\kappa}{\mathrm{d}t} + \kappa = \frac{1}{2}f\cos\Phi \qquad \tau\kappa\frac{\mathrm{d}\psi}{\mathrm{d}t} = \frac{1}{4}f\sin\Phi. \tag{3}$$

Note that the formal solution can be written for the two last equations in (3) and this system can be represented as an integrodifferential equation for $\varphi(t, \boldsymbol{r})$:

$$\frac{\alpha}{c^2}\frac{\partial^2\varphi}{\partial t^2} - \alpha\nabla^2\varphi + \lambda\frac{\partial\varphi}{\partial t} + \frac{\partial w_a}{\partial\varphi} = f\boldsymbol{L}\{\varphi(t)\}$$
$$\boldsymbol{L}\{\varphi(t)\} = f\int(\mathrm{d}t'/\tau)\exp[(t'-t)/\tau]\sin(2[\varphi(t)-\varphi(t')]). \tag{4}$$

Let us estimate the magnetic parameters entering the equations (3) and (4). The magnitude of the essential crystal anisotropy is determined by the anisotropy field $H_6 = 3\beta_6 M_0 \approx 0.26$ Oe. The uniaxial compression in a basal plane is often used to create a stripe-domain structure in $FeBO_3$ inducing a rhombic anisotropy with a constant β_2. This anisotropy field H_2 may reach some Oe [10].

The PUMA constant magnitude is defined by the field $H_f = fM_0$. According to [6, 7], pure $FeBO_3$ has a value of $H_f \leqslant 0.1$ Oe, and for $FeBO_3$:Ni it reaches 1.5 Oe [12] which is greater than H_6. The constant τ is equal to 10^3 s at $T = 100$ K and the radiation intensity I is about 0.1 W cm^{-2}. The value of τ is inversely proportional to I, $\tau \sim 1/I$ [12] for a wide range of I. The value of the relaxation constant λ for a slow magnetization dynamics is unknown, so let us assume that the dimensionless constant $gM_0\lambda \sim 1$ according to the observed autowave parameters [1–3].

The simplest analysis of equations (3) or (4) can be performed for rather slow-changing magnetization when $\tau(\mathrm{d}\varphi/\mathrm{d}t) \ll 1$. As we shall be convinced further this condition is not realized in the experimentally observed autowave. However, the investigation of the $\varphi(t)$ dynamics in this limit is useful for a more transparent representation of the unusual properties of the system. To first order in $\tau(\mathrm{d}\varphi/\mathrm{d}t)$ the integral operator on the right-hand side of equation (4) is transformed into a differential one, $\boldsymbol{L}\{\varphi(t)\} \to \tau(\mathrm{d}\varphi/\mathrm{d}t)$. It is clear that in this case PUMA leads to a renormalization of the relaxation constant $\lambda \to \lambda_{eff} = \lambda - 2f\tau$. Thus, if $f > 0$, the effective relaxation constant for rather slow oscillations becomes negative at $2f\tau/\lambda > 1$. Even at $gM_0\lambda \sim 1$, this inequality for $FeBO_3$ (also for $FeBO_3$:Ni) is fulfilled with a great reserve (see above).

With increasing of the frequency ω, the simple substitution of $\boldsymbol{L}\{\varphi(t)\} \to (\mathrm{d}\varphi/\mathrm{d}t)$ becomes inadequate, i.e. $\lambda_{eff} = \lambda_{eff}(\omega)$. To investigate the stability of a homogeneous state we shall linearize (3) according to φ. The solution has the form $\varphi = \varphi_0 \exp(\mathrm{i}\omega t - \mathrm{i}\boldsymbol{k}\boldsymbol{r}_\perp - \Gamma t)$, where the parameters Γ, $k = |\boldsymbol{k}|$ and ω are connected by the formulae

$$\frac{\alpha}{c^2}\Gamma = \lambda - \frac{2f\tau}{\omega^2\tau^2 + (\tau\Gamma - 1)} \tag{5}$$

$$\frac{\alpha}{c^2}(\omega^2-\Gamma^2)+2f\frac{(\omega\tau)^2+\tau\Gamma(\tau\Gamma-1)^2}{\omega^2\tau^2+(\tau\Gamma-1)^2}=b-\lambda\Gamma \tag{6}$$

where the constant b, which has the sense of an effective stiffness constant for the wave with wavevector $\boldsymbol{k}$, $k=|\boldsymbol{k}|$, is introduced,

$$b\equiv b(k)=n\beta_n+\alpha k^2. \tag{7}$$

From (5) it follows that at $f<0$ one has $\Gamma>0$, and any initial perturbation is decaying. If the PUMA constant $f>0$, then for excitations with frequency $\omega<\omega_c$, $\omega_c=(1/\tau)(2f\tau/\lambda-1)^{1/2}$, one has $\Gamma<0$, i.e. the homogeneous state with $\varphi=0$ is unstable.

The estimation of ω_c, with account being taken of the specific parameter values, gives $\omega_c\leqslant 10^2\ \mathrm{s}^{-1}$. The autowave frequency is of the same order or smaller (see later). The term with $(\alpha/c^2)(\omega^2/\beta)\sim\omega^2/\omega_{afr}^2$ is rather small (the antiferromagnetic resonance frequency ω_{afr} for $FeBO_3$ exceeds $10^{11}\ \mathrm{s}^{-1}$) and the terms with the second time derivatives in (3) and (4) may be omitted. The omission of the $\partial^2\varphi/\partial t^2$ term in (6) gives the simple formula for the instability increment $(-\Gamma)$ of the wave with wavevector $\boldsymbol{k}$:

$$(-\Gamma)=\frac{f}{\lambda}-\frac{1}{2\tau}-\frac{b(k)}{2\lambda}. \tag{8}$$

This formula is too transparent from the physical viewpoint. The homogeneous state is unstable at a rather large PUMA constant $f>f_c$ or at small anisotropy $b<b_c$. Thus, on the plane (b,f), the instability region of the homogeneous ground state is on the right of the curve

$$\frac{2f\tau}{\lambda}=1+\frac{b\tau}{\lambda} \tag{9}$$

see figure 1. By decreasing the effective constant b (for example, by decreasing the external magnetic field H or the β_2 constant of the induced rhombic anisotropy) from the values above the curve, the system may reach the instability region where the autowaves occur.

Let us write the simplest version of the equation which is adequate for the analysis of the problem in spatially homogeneous oscillations. Omitting the terms with $\partial^2\varphi/\partial t^2$, and $\nabla^2\varphi$, using the dimensionless variable $X=2\kappa/f$ and parameters $B=b\tau/\lambda=n\beta_n\tau/\lambda$ and $F=2f\tau/\lambda$, one can easily get

$$\tau\frac{\mathrm{d}X}{\mathrm{d}t}+X=\cos\Phi\qquad\tau\frac{\mathrm{d}\varphi}{\mathrm{d}t}=\frac{1}{2X}\sin\Phi\qquad\tau\frac{\mathrm{d}\varphi}{\mathrm{d}t}=\frac{X}{2}F\sin\Phi-\frac{1}{n}B\sin n\varphi. \tag{10}$$

So the set of equations (3) in the homogeneous case can be represented in a form equivalent to the dynamical system with 3/2 degrees of freedom. It is well known that such equations are of rather non-trivial behaviour [11].

3. Small-amplitude autowaves

The set of equations for the variables φ, Φ, κ or φ, ψ, κ gives way to rather full investigation for small-amplitude (weakly-nonlinear) autowaves when deviations of the variables from their equilibrium value are small, $\varphi\ll 1$, $\psi\ll 1$ and $f/2-\kappa\ll f/2$. Let us consider the properties of weakly-nonlinear autowaves for various types of anisotropy (the cases of $n=6$ and $n=1$ were discussed in [8]).

Let us seek the solution in a simple autowave form when all variables depend on a coordinate and time through the combination $\omega t-\boldsymbol{k}\boldsymbol{r}_\perp$; ω and $\boldsymbol{k}$ are the autowave frequency and wavevector, respectively. To build a solution, the asymptotic procedure, see

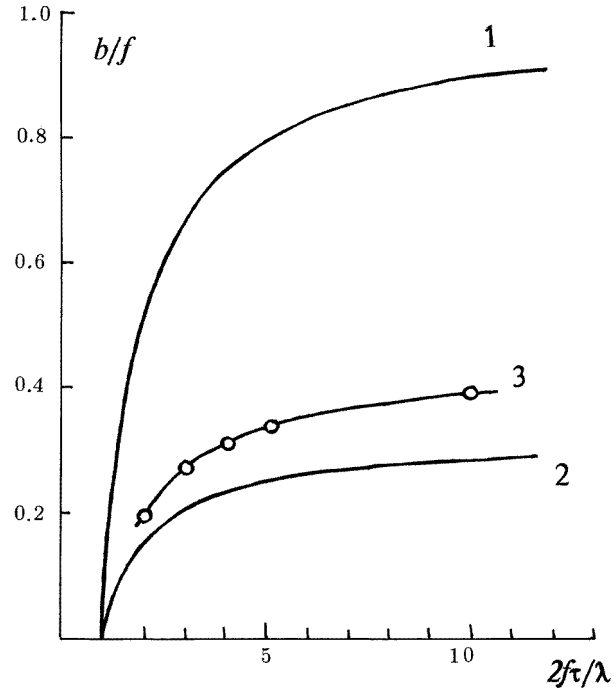

Figure 1. The region of stability and instability (above and below the curve 1, respectively) of the homogeneous ground state. This figure also shows another bifurcation line: the line of the limit cycle 'opening' $B = B_0(F)$, curve 2, and the line of the new (long) limit cycle creating $B = B_1(F)$, curve 3, see below section 6. Open cycles are the result of numerical calculation.

[13], was used. According to this procedure the solution has to be expanded by harmonics, for example

$$\Phi = A\cos(\boldsymbol{kr}_\perp - \omega t) + A_3\cos(3\boldsymbol{kr}_\perp - 3\omega t) + A_5 + \cdots \tag{11}$$

where A is the amplitude of the autowave, $A \ll 1$; the coefficients A_3, A_5, ... are proportional to the next powers of the amplitude, $A_n \propto A_n$.

After a simple but cumbersome algebra we can construct a solution exact to any order in the autowave amplitude, which is the smallest parameter of the method. To first order in amplitude the solution can be easily found by taking account of (11):

$$\begin{aligned}
&\psi = (1/\omega\tau)\sin(\omega t - \boldsymbol{kr}_\perp)\\
&\varphi = (A/2)[1 + (1/\omega\tau)^2]^{1/2}\cos(\omega t - \boldsymbol{kr}_\perp - \arctan(1/\omega\tau))\\
&\kappa = \frac{f}{2}\left\{1 - \frac{A^2}{4} - \frac{A^2}{4}\frac{1}{[1+4(\omega\tau)^2]}\cos(2\omega\tau - 2\boldsymbol{kr}_\perp)\right\}.
\end{aligned} \tag{12}$$

The relationship between the amplitude A, frequency and wavevector is obtained from the condition of the exclusion of the secular terms [13] up to A^3 and can be written as follows:

$$\begin{aligned}
\frac{2f\tau}{\lambda} - 1 - \frac{\tau b}{\lambda} = {} & \frac{A^2}{8}\left(\frac{2f\tau}{\lambda} + 1\right)\left[2 + \frac{1}{1+4(\omega\tau)^2}\right]\\
& + \frac{A^2}{8}\frac{n\beta_n\tau}{\lambda}\left[1 - \frac{n^2}{4} - \frac{n^2}{4(\omega\tau)^2} - \frac{1}{1+4(\omega\tau)^2}\right]
\end{aligned} \tag{13}$$

$$\omega^2 = \frac{b}{\lambda\tau} + \frac{A^2}{4}\left(\frac{2f\tau}{\lambda}+1\right)\frac{\omega^2}{1+4(\omega\tau)^2} + \frac{A^2 n\beta_n}{8\lambda\tau}\left\{1-\frac{n^2}{4}-\frac{n^2}{4(\omega\tau)^2}+\frac{1}{1+4(\omega\tau)^2}\right\} \tag{14}$$

where $b = b(k)$, see equation (7), is the effective stiffness constant.

First, it is necessary to note that according to (8) the instability develops for the smallest value of the effective constant b. For the considered model it corresponds to $k = 0$, i.e. the homogeneous auto-oscillations are excited. However, in a real case of a magnetic plate of finite thickness L the magnetic dipolar interaction leads to the minimum of $b(k)$ at a finite value of $k = k_0$ (it was shown in [14–16] in connection with the theory of domain structures). In the weakly-nonlinear wave approximation it is also possible to consider more general models. We dwell on the account of the magnetic dipolar interaction, which (from our point of view) forms the period of the space unhomogeneities observed in [1–3].

The occurrence of the inhomogeneities is connected with the contribution of a rather small component m_{0z} of the magnetic moment and therefore the account of this interaction can be taken in the linear approximation only. The magnetic dipolar interaction leads to an additional term in (1):

$$F_m = -(\delta/\delta\varphi)\int (\boldsymbol{M}\boldsymbol{H}_m)\,\mathrm{d}\boldsymbol{r}.$$

Here $\boldsymbol{H}_m$ is known as the demagnetizing field, which is determined by the magnetostatic equations [17],

$$\mathrm{div}\boldsymbol{H}_m + 4\pi\,\mathrm{div}\boldsymbol{M} = 0 \qquad \mathrm{rot}\boldsymbol{H}_m = 0 \tag{15}$$

with account being taken of the usual boundary conditions of a continuity of the normal components of the magnetic induction $\boldsymbol{B} = \boldsymbol{H}_m + 4\pi\boldsymbol{M}$ and the tangential component of the magnetic field $\boldsymbol{H}_m$ [17]. The solution of equations (1) and (15) inside and outside of the plate has been searched for as the combination of exponents such as

$$\exp\{\mathrm{i}\omega t - \mathrm{i}\boldsymbol{k}\boldsymbol{r}_\perp - \mathrm{i}qz\}.$$

Here $\boldsymbol{r}_\perp$ and the values $q = \pm q_\alpha$, $\alpha = 1, 2, 3$, are determined by the boundary conditions for B_n and $(\boldsymbol{H}_m)_t$, as well as the condition for the magnetization $(\partial\boldsymbol{M}/\partial z)|_{z=\pm L/2}$, see the details of the calculations in [15, 16].

It is possible to show that the orientation of $\boldsymbol{k}$ parallel to the equilibrium direction of the magnetization in the basal plane corresponds to the minimal value of the spin wave frequency at a given $k = |\boldsymbol{k}|$. This means that such a wave will be responsible for the loss of stability of the homogeneous ground state. This prediction is in agreement with experiment [1–3]. It has been observed that an autowave with $\boldsymbol{k}$ parallel to the external magnetic field $\boldsymbol{H}$ occurs. When $\boldsymbol{H} = 0$ and the domain structure appears, three systems of autowaves with different directions of $\boldsymbol{k}$ are realized. These directions are parallel to the magnetization of each domain [1]. For a sufficiently thick plate, $L \gg \sqrt{\alpha}/m_{0z}$ (in experiments [1–3] this inequality is fulfilled with a large stock), it can be shown that the condition for continuity of B_n is most important and it is possible to take into account only one (smallest) value of q, see [15, 16]. The relation between this value of q and k can be expressed by a simple formula $q/k = \tan(qL/2)$. For the frequency $\omega(k)$ it is easy to get the expression

$$\omega^2 = \omega_0^2 + c^2\{(k^2+q^2) + 4\pi q^2(m_{0\perp})^2/\alpha(k^2+q^2)\}$$

where ω_0 is the frequency with $k = 0$ and without account being taken of the magnetic dipolar interaction.

Analysis shows that, near the minimum of the function $\omega = \omega(k)$, $q \gg k$ and $qL \cong \pi$. From here, it follows that the minimum of the frequency is observed at $k = k_c$,

$$k_c = (\pi^3 m_{0z}^2/\alpha L^2)^{1/4}.$$

A specific calculation has shown that real magnitudes of α, m_{0z} and the plate thickness L lead to a $1/k_0$ value equal to 100 μm, which corresponds to the experimentally observed autowave period [1–3].

In papers [8, 18] it was also noted that it is possible to distinguish the reasons for the occurrence of the instability and the formations of the inhomogeneities, which have dissipative and dynamic characters, respectively. However, the authors of [18] offered another source for the occurrence of the inhomogeneities, namely, a magnetoelastic interaction. From their approximate formula for the frequency of the magnetoelastic wave, it follows that this minimum exists at some non-zero value. On the other hand, such a minimum is not present in the exact theory of magnetoelastic waves, see formulae (3.13) and (3.14) of the review article [19].

Let us discuss the weakly-nonlinear autowave properties. According to (13), the amplitude A becomes zero on a critical line (9), i.e. at $f \to f_c$ or $b \to b_c$, where

$$\frac{b_c}{f} = 1 - \frac{\lambda}{2f\tau}$$

the magnitude $\omega^2 \approx \omega_c^2$ being equal to $n\beta_n/\lambda\tau$. According to the logic of the asymptotic procedure, one can consider the amplitude A and magnitudes $\omega^2 - \omega_c^2$ and $\beta - \beta_c$ to be the smallest problem parameters. Then, in the terms proportional to A^2 one could change β to β_c and ω to ω_c. As a result, equation (13) can be written as follows (here $B_c = 2f\tau/\lambda - 1$):

$$\frac{b_c - b}{b_c} = \frac{A^2}{8}\left\{3 - \frac{n^2}{4} + \frac{4 - n^2/4}{B_c} + \left(\frac{2}{B_c} - 1\right)\frac{1}{(1 + 4B_c)}\right\}$$
$$\to \frac{A^2}{8}\begin{cases} 3 - n^2/4 & B_c \gg 1 \\ (6/B_c)(1 - n^2/24) & B_c \ll 1 \end{cases}. \tag{16}$$

From these equations it follows that for small values of b_c, i.e. for $(2f\tau/\lambda - 1) \ll 2f\tau/\lambda$ and at $n < 6$, the sign of $b_c - b$ is positive, and the amplitude is determined by the formula

$$A = \begin{cases} 0 & b > b_c \\ \sqrt{C(b_c - b)/b_c} & b < b_c \end{cases} \tag{17}$$

where C is a positive constant.

This form is standard for the so-called soft excitation of autowaves [11]. If $b_c \gg \lambda/\tau$, i.e. $2f\tau/\lambda \gg 1$ (this limiting case corresponds to the $FeBO_3$:Ni parameter values in experiments [1–3]), the coefficient on the right-hand side of (16) is positive only for $n^2 < 12$, i.e. for the magnetic field ($n = 1$) and for the rhombic anisotropy ($n = 2$) cases. Soft excitation and a dependence like (17) are also realized in these cases. If $n = 4$ or 6, equation (16) has a solution only at $b > b_c$, i.e. in the homogeneous state stability region. This situation is characteristic of the so-called hard excitation when $b_c < b < b_\perp$ and the homogeneous state is stable but there are two finite limit cycles describing the autowave. One of these limit cycles determined by equation (16) is unstable and the other, with an amplitude which never becomes zero, is a stable one. There is only one stable cycle at $b < b_c$. In general, the analysis of this problem may also be carried out through the asymptotic procedure (for $n = 6$ this has been performed in [8]), but it requires very cumbersome calculations (up to fifth order in A). A soft excitation was observed in the experiment and we shall limit ourselves to this case.

As we have already noted, the soft excitation is realized for rhombic anisotropy ($n = 2$). For $n = 4$ and 6, this excitation takes place only in the presence of a rather large magnetic field. For the autowave frequency ω it is easy to obtain formulae like $\omega_c^2 - \omega^2 \propto \omega_c^2 A^2$, for example, at $B_c \gg 1$

$$\omega^2 = \omega_c^2\{1 - (3A^2/8)(1 - n^2/24)\} = \omega_c^2\{1 + (b - b_c)/b_c\}. \tag{18}$$

Usually for the soft excitation case the autowave frequency decreases with increasing amplitude. The analysis of weakly-nonlinear oscillations predicts a linear dependence between ω^2 and A^2 like $\omega^2 = \omega_c^2\ (1 - A^2/A_0^2)$. This agrees with experiments [2, 3] at small amplitudes.

4. Rotational dynamics of magnetization

A rather detailed analysis is possible in another limiting case when $f \gg \beta$. An exact solution of equations (10) can be found if one completely neglects the magnetic anisotropy. There is no angle φ in these equations and the dynamics of κ and Φ is determined by the set of two equations

$$\tau\frac{\mathrm{d}\kappa}{\mathrm{d}t} + \kappa = (f/2)\cos\Phi \qquad \tau\frac{\mathrm{d}\Phi}{\mathrm{d}t} = (4\kappa\tau/\lambda - f/2\kappa)\sin\Phi. \tag{19}$$

Solving these equations, it is easy to find the time dependence of the angles ψ or φ from the formulae $\tau(\mathrm{d}\psi/\mathrm{d}t) = (f/4k)\sin\Phi$, $\varphi = \psi + \Phi/2$.

The analysis of system (19) can be carried out through the phase plane method. It is easy to see that, at $2f\tau/\lambda \leqslant 1$, only one type of singular point

$$\Phi = \pi m \qquad k = (f/2)(-1)^m \qquad m = 0, \pm 1, \pm 2$$

which are stable focuses, corresponding to a ground state $\varphi = \psi + \pi m$, $\varphi = \psi = 0$, is present. If $2f\tau/\lambda > 1$, these singular points become saddle points and loose their stability, but the stable focuses at

$$\Phi = \pi m \pm \Phi_0 \qquad \kappa = \kappa_0 = (f/2)(-1)^m\cos\Phi_0 \qquad \cos\Phi_0 = (\lambda/2f\tau)^{1/2} \tag{20}$$

appear in the system. These states correspond to growth, which is linear with time, of the angles φ and ψ,

$$\frac{\mathrm{d}\psi}{\mathrm{d}t} = \frac{\mathrm{d}\varphi}{\mathrm{d}t} = \omega_0 = (1/2\tau)\tan\Phi_0 = \frac{1}{2\tau}\sqrt{\frac{2f\tau}{\lambda} - 1}. \tag{21}$$

Thus at $\beta = 0$ and $2f\tau/\lambda > 1$ the homogeneous synchronized precession of the magnetization and the PUMA axis with frequency ω_0 takes place in the magnet. The angle between them has a constant value of $\Phi_0/2$. Correction to this solution may be found at small but finite values of β_n/f, for example

$$\begin{aligned}\kappa &= \kappa_0 - \frac{\beta}{2}\sqrt{\frac{2f\tau}{\lambda}}\,\frac{n\cos n\omega t + \omega\tau(n^2 - 8)\sin n\omega t}{n^2 + (8 - n^2)\omega^2\tau^2}\\ \varphi &= \omega t + \frac{2\beta\tau/\lambda}{\sqrt{(2f\tau/\lambda - 1)}}\,\frac{2(4 - n^2)\omega\tau\sin n\omega t + n[1 + (8 - n^2)\omega^2\tau^2]\cos n\omega t}{n^2 + (8 - n^2)\omega^2\tau^2}\end{aligned} \tag{22}$$

where k_0 and $\omega \equiv \omega_0$ are defined by the formulae (20) and (21).

Thus, taking account of small but finite anisotropy causes additions to κ, φ and ψ which are proportional to b and have harmonic time dependence like $a\cos\omega t + b\sin\omega t$. Consequently, a stationary point $\Phi = \Phi_0$, $\kappa = \kappa_0$ on the (Φ, κ) plane (see equation (20)) must transform into a limit cycle. Numerical integration of the equation of motion at small

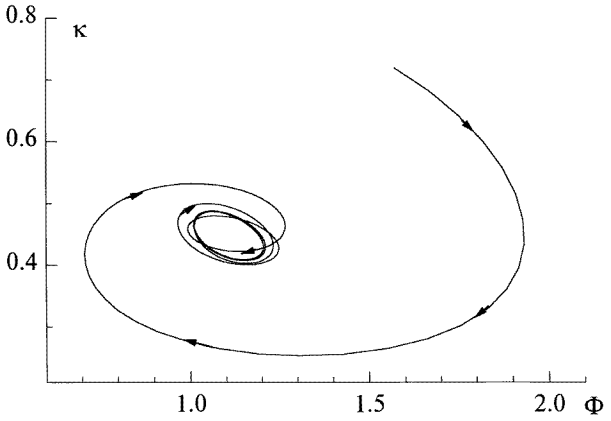

Figure 2. The phase trajectory projection of system (4) on the (Φ, φ) plane, $n = 2$, $2f\tau/\lambda = 5$, $b/f = 0.02$.

b/f approves this result, see figure 2. This analysis also shows that this cycle is absolutely stable. Phase trajectories quite quickly reached the limit cycle at different initial conditions corresponding to the phase-space points lying both far from the cycle and inside it.

Note also that similar 'open' trajectories correspond to periodic motion of the magnetization $\boldsymbol{m}$. In particular, the Φ and κ dependence on $m_x = \sin\varphi$ or $m_y = \cos\varphi$ are described by closed curves (see figure 8 later) in all the regions in which the open trajectories exist.

5. Large-amplitude oscillations. The picture of bifurcations

The analytical solution of equations (3) or (10) may be found at two limiting cases: when b is close to b_c, i.e. $b \approx 2f - \lambda/\tau$ and when $b \ll f$. These cases have considerably different solutions. They correspond either to a small-amplitude autowave or to a wave with rather large amplitude with magnetization rotation in the basal plane. The investigation of the intermediate region with parameters $b_0 - b \sim b_c$ can be performed numerically only.

Numerical analysis of auto-oscillations described by the system (10) was made for two of the most interesting physical models: the magnet with rhombic anisotropy ($n = 2$) and the magnet in the presence of the magnetic field $\boldsymbol{H}$ oriented in a basal plane ($n = 1$). The dimensionless parameters $B = n\beta_n\tau/\lambda$ and $F = 2f\tau/\lambda$ are used.

Preliminary analysis consisted of the solution of the Cauchy problem for the set of two equations for phase trajectories $\kappa = \kappa(\varphi)$ and $\Phi = \Phi(\varphi)$. Also the stationary solutions at various initial conditions and parameters of the problem were investigated. For the investigation of the real time dependence of the parameters κ, Φ and φ the set of three equations (10) was solved and a special program for the limit-cycle search was used (see later). The numerical integration was performed by the fourth-order Runge–Kutta method.

The analysis did not show qualitative differences of the results for the given models; therefore we shall discuss them simultaneously. In all cases the functions $X = X(\varphi)$ or $\Phi = \Phi(\varphi)$ describing stationary motion were periodic at $B < B_0$ and were determined by close curves at $B > B_0$. Thus, in the first stage we have found the first bifurcation: the transition from periodic magnetization oscillations to rotational motion. This transition may be called the 'opening' of the limit cycle. The values of the bifurcation parameters

$B_0 = B_0(B/F)$ are shown in figure 1. Further increase of F (up to 10^3) leads to saturation of this dependence.

At $B_0 < B < B_c$ we observed only closed trajectories in the planes (X, φ) and (Φ, φ) corresponding to periodic oscillations (limit cycles). (A periodic system of cycles differing by the shift $\varphi \to \varphi + \pi m$, $\psi \to \psi + \pi l$, where l, m are integer, should be observed). At rather large $B \leqslant B_c$, i.e. in the case of weak nonlinearity of the oscillations, the curves $\Phi(\varphi)$ or $\psi(\varphi)$ were close to ellipses. The limit-cycle form changed considerably when decreasing B from B_c to B_0. The curves were more complicated at smaller values of B.

At $B \leqslant B_0$ the transition from closed to open trajectories (the 'opening' of the limit cycles) was observed. In the (Φ, φ) plane this transition looks like limit-cycle breaking along the line $\Phi = 0$. Open trajectories may be formed from up or down parts of the cycles, see figure 3. At $B - B_0 \ll B_0$ and initial conditions close to the limit cycle, the point in the phase space (depicting point) can move for a long time along this cycle, and the time of this transition sharply increases.

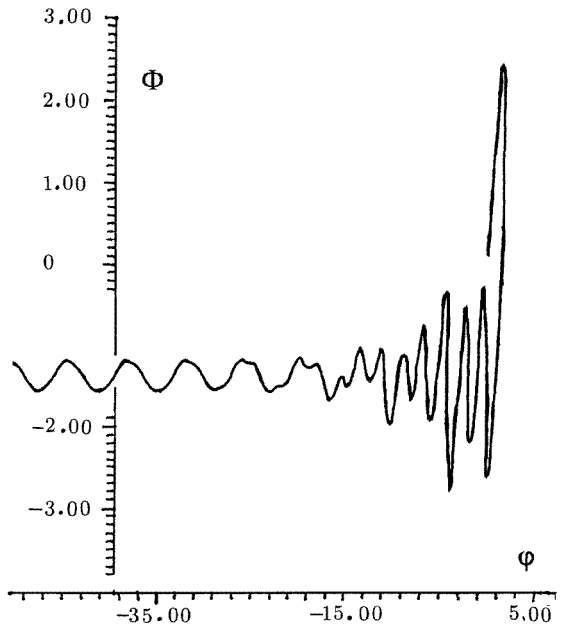

Figure 3. The projection of the phase trajectory on the (Φ, φ) plane at $n = 1$, $F = 5$, $B/F = 0.248$. The beginning of the trajectory is close to a limit cycle existing at $B/F = 0.25$. Then the depicting point goes to the trajectory corresponding to the oscillations of Φ around $-\pi/2$ and the infinite growth of φ.

Analysis of the real time dependence of the variables was made by using a special program of limit-cycle investigation. The solution of the set of equations (10) determines the motion of the point in a three-dimensional (X, φ, ψ) phase space. The limit cycle corresponds to a closed trajectory. The initial point $X = X^{(0)}$, $\varphi = \varphi^{(0)}$ was chosen in a plane $\psi = 0$. Then the set of equations was numerically integrated until the phase trajectory crossed the plane $\psi = 0$ the next time. This crossing, generally, took place at different points $X_1 = G(X^{(0)})$, $\varphi_1 = \Theta(\varphi^{(0)})$, with the position depending on the initial values of X and φ. Furthermore, the set of algebraic equations,

$$X = G(X) \qquad \varphi = \Theta(\varphi)$$

describing the closing of the phase trajectory, was solved by using a standard numerical Newton method program. This solution gave values of the initial states at which the phase trajectory in space X, φ, ψ had the shape of a closed curve describing a limit cycle.

Note that both stable and unstable limit cycles can be found by means of this procedure. That is why the limit-cycle stability investigation of equation (10), with initial conditions close to the limit cycle, is an important topic for further analysis. The stability was defined by a deviation growth δ_n,

$$\delta_n = [(\varphi_n + 1 - \varphi_n)^2 + (X_{n+1} - X_n)^2]^{1/2}.$$

Here φ_n and X_n are the values of φ and X at the nth crossing of the plane $\psi = 0$. These calculations were rather prolonged and were performed for $n = 2$ and some chosen values of $F = 2f\tau/\lambda$.

The analysis has shown that the closing of the trajectory (with a given relative precision 10^{-4}) was realized only at $B > B_0$ where $B_0 = B_0(F)$ is a bifurcation value corresponding to the above-described transition to rotational motion. The period T of the limit cycle increases with decreasing B (see figure 6 later), i.e. T increases (frequency $\omega = 2\pi/T$ is decreasing) with increase of the amplitude A. Note that this is typical for soft autowave excitation. At small A the frequency value is close to the one found in the small-amplitude approximation, $\omega \to \omega_c = (b/\lambda\tau)^{1/2}$ and $\omega_c T \to 2\pi$.

We observed an interesting phenomenon when decreasing B for all values of F. New limit cycles with a period more than twice as large (the 'long' limit cycle, in contrast with the 'short' one considered above), see figure 4, appear at $B \leqslant B_1$. The corresponding bifurcation value $B = B_1(F)$ is plotted above in figure 1.

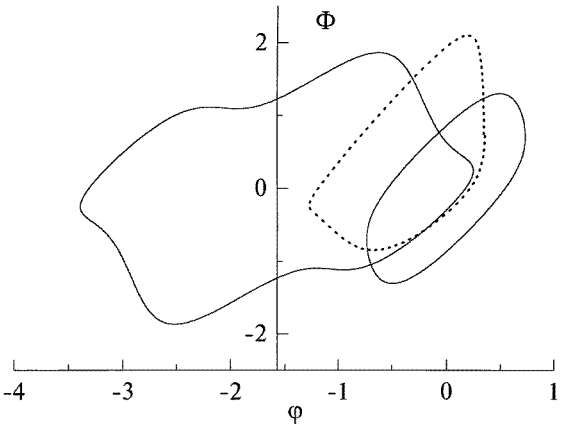

Figure 4. The projections of 'long' and 'short' limit cycles on the (Φ, φ) plane for $n = 2$, $F = 5$, $b/f = 0.372$ near the centre of the region of long-cycle appearance. The dotted line shows the unstable limit cycle, see below.

One can easily see that this phenomenon is not the usual period doubling typical for many nonlinear systems [11]. The phase trajectories of short and long limit cycles have a very strong difference. No part of the trajectories coincide. The program searches for one or another limit cycle depending on the initial φ and κ values used. When B values are rather close to B_1 both cycles are stable. That is, a depicting point (initial deviation $\delta \leqslant 10^{-6}$) preserved the deviation of $\delta \leqslant 10^{-5}$ during more then 1000 cycles (5×10^5 steps by the Runge–Kutta scheme). At this stage we did not succeed in finding other limit cycles (in particular, unstable) at $B \leqslant B_1$.

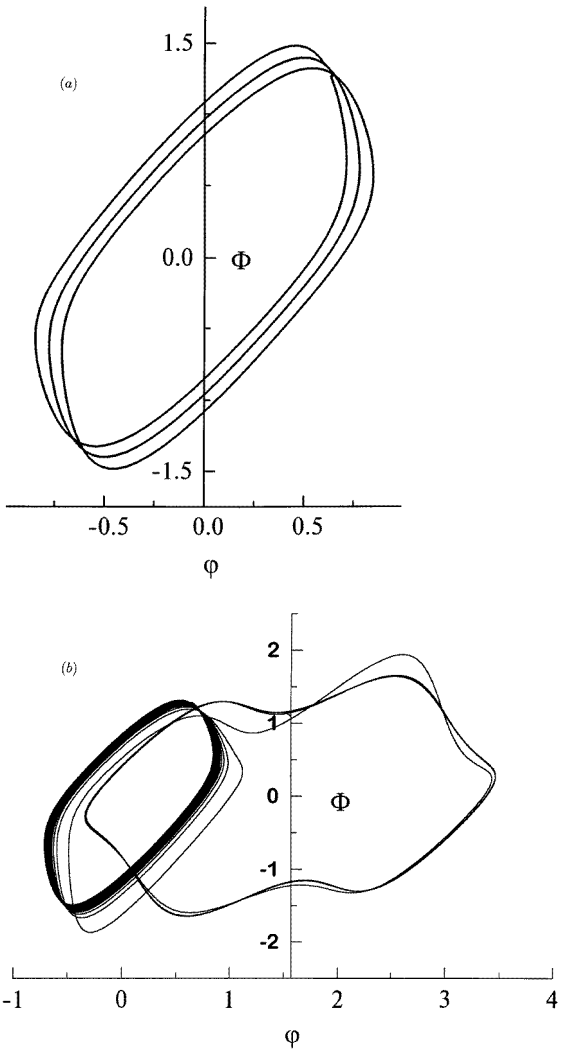

Figure 5. The phase trajectories at $F = 5$, $B/F = 0.324$. (a) Limit circles (the stable cycle in the middle, and two unstable cycles); (b) the trajectory leaving from the right limit cycle to the long limit cycle with central point near $\varphi = \pi/2$.

An occurrence of a new single limit cycle is a quite extraordinary phenomenon for the dynamic system. The systems with limit cycles with one degree of freedom occur in pairs only. One of the cycles in the pair is stable and the other is unstable. For systems with more than one degree of freedom the occurrence of the single cycle is not restricted but as far as we know it has not been observed earlier.

We have performed more detailed investigations at $F = 5$ to clarify limit-cycle bifurcations. We have also found unstable limit cycles. Note that this was not an easy task as their instability increment is quite small for only a narrow interval of B values (δ_n increased by a factor of 10 for $n = 30$, 12 and 5 at $B/F = 0.324$, 0.328 and 0.332, respectively). At greater B values the increment is rather large and unstable limit cycles manifest themselves only for transition processes.

Let us describe bifurcations of the periodic solutions of equations (4) at $B_0 < B < B_1$. In order to do this one must take into account the periodic set of both long and short limit cycles. They differ from one another by a shift in φ and ψ at πn.

Consider a stable short limit cycle with central point at $\varphi = 0$, $\varphi = 0$. We have found two well defined unstable limit cycles close to this stable one at $0.324 \leqslant B/F \leqslant 0.33$, see figure 5($a$). The system reaches the short stable cycle when the initial value lies inside a small region occupied by them. The phase trajectory behaviour is quite different if the initial point is out of this small region. Phase trajectories beginning on the 'right' and on the 'left' from 'right' and 'left' unstable cycles tend to two different but equivalent long cycles, with centres at $\varphi = \pi/2$, $\psi = 0$, see figure 5(b), and $\varphi = -\pi/2$, $\varphi = 0$, respectively.

Unstable limit cycles move away from short stable cycles with B/F growth, see figure 4, and their periods and increments sharply increase. This fact made their search too complicated. However, one can observe that at $B \to B_1$ these unstable cycles are close to two long stable ones. This fact can be easily seen from figure 6 which demonstrates the dependence of the limit-cycle period on B.

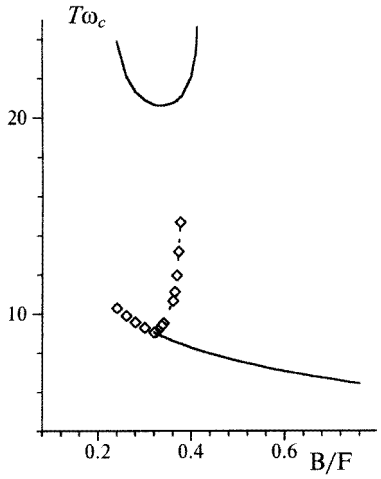

Figure 6. The dependences of the periods T of the limit cycles (in units of $1/\omega_c$, ω_c is the frequency of the small-amplitude oscillations) on $B/F = \beta_2/f$ for $n = 2$, $2f\tau/\lambda = 5$. Full lines represent the dependences for stable cycles, diamonds represent those for unstable ones.

Thus the bifurcation at B_1 can be described as the occurrence of the set of pairs of new limit cycles: a stable long cycle and a unstable one with a great instability increment. Unstable cycles linked with neighbouring long cycles (for example, centred at $\varphi = \pi/2$, $\psi = 0$ and $\varphi = -\pi/2$, $\psi = 0$) move quickly to a stable short cycle (centred at $\varphi = \pi/2$, $\psi = 0$) as B decreases to the value $B/F = 0.324$ at $F = 5$. Then two unstable cycles coincide with a short stable one; we could not separate them at a given accuracy of 10^{-4}. Moreover, even if a stable short cycle exists, the initial-condition region leading to it is quite narrow. This three-cycle junction manifests itself as an unstable short cycle, with a very small instability increment. Thus there is only one stable limit cycle (the long one) at $B_0 < B < B_2$, $B_2/F = 0.324$ at $F = 5$. However, short cycles can also be observed at $B < B_2$ at a time of less than 100 periods.

One can also point to an initial-condition region leading to 'open' trajectories for the same values of the parameters. The transition from a limit cycle to open trajectories describing periodic magnetization motion with a full reverse in a basic plane begins at

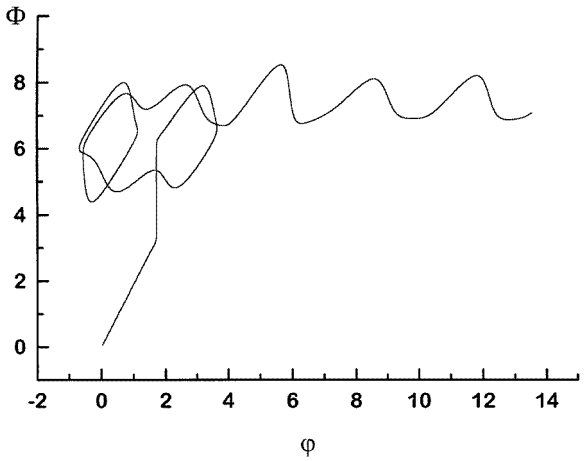

Figure 7. The transition to the magnetization precessional motion at $2f\tau/\lambda = 5$, $B = 0.98B_0$.

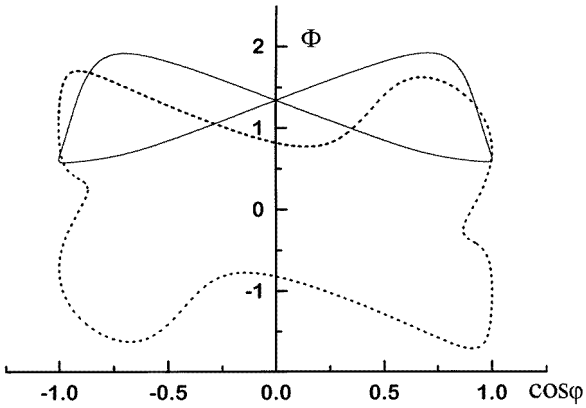

Figure 8. Phase trajectories on the $(\cos\varphi, \Phi)$ plane at $2f\tau/\lambda = 5$, $B = B_0$. The full line describes the rotational motion, the dotted line the long limit cycle.

$B < B_2$. At $B < B_0$ only open trajectories exist. This transition may be described as long-limit-cycle destabilization. Besides the transition process at $B \leqslant B_0$, the depicting point can perform some revolutions around unstable cycles, both long and short, see figure 7. Note that the 'open' phase trajectories are closed for physical variables Φ and κ, and $m_x = \sin\varphi$ or $m_y = \cos\varphi$, see figure 8. Thus auto-oscillation of the magnetization vector $\boldsymbol{m}$ is periodic in the whole region $0 < B < B_c$.

6. Conclusion

The theory developed in this paper allows us to explain the magnetization auto-oscillation and autowaves observed in [1–3]. They are a consequence of an anomalous photo-induced anisotropy in $FeBO_3$ with nickel or some other impurities under the action of radiation. Not all the experimental details can be described quantitatively by our theory. However, there is a most important phenomenon in this theory, which is adequate to describe the experimental

evidence: the appearance of auto-oscillations with a frequency of the order of 10–100 Hz, which is significantly less than the frequency of the linear antiferromagnetic resonance. The auto-oscillation frequency values which were calculated according to PUMA parameters defined from independent experiments have been in good agreement with experimental data. However, the analysis we have carried out has shown that with amplitude growth the auto-oscillation character becomes more complicated than observed in [1–3].

The experiments [1–3] were performed using one type of sample only, namely, thin films with the presence of growth-induced in-plane rhombic anisotropy. The magnetic dipolar interaction also plays a significant role in these samples, forming a domain structure at small fields. Only space inhomogeneous auto-oscillations of quite small amplitude ($\Delta\varphi < 10^\circ$) were observed in these samples. To our mind, it is of great interest to investigate the photo-induced auto-oscillations in $FeBO_3$:Ni-like materials in conditions where the strongly nonlinear auto-oscillations take place. In this situation bifurcation like 'short cycle'–'long cycle'–'open trajectories', describing a transition from oscillation around the value $\varphi = 0$ to that around the value $\varphi = \pi/2$ and then to magnetization rotation, should be seen. Our calculation showed that this set of bifurcations took place at a reasonable value of the ratio of the anisotropy and the PUMA constants, namely at $0.6 < \beta_2/f < 1.03$, which can be realized for $FeBO_3$:Ni. The moderation of the role of the magnetic dipole interaction, which takes place for small enough spherical samples, is probably also important.

The magnetization auto-oscillation with unique properties (large amplitude, low frequencies and the presence of multistability) can be realized if such conditions are fulfilled. Note that great attention has been paid to chaotic auto-oscillation and controlled chaos phenomena, see, for example, [20–22]. We did not observe the chaotic behaviour of auto-oscillations in the frame of system (4). Nevertheless, it is quite probable that the appearance of chaotic auto-oscillation in the multistability region ($B_0 < B < B_1$) may occur with the presence of small enough pumping. The suppression of such chaotic auto-oscillation during the changing of the parameter values is also possible. From the point of the general physics of nonlinear oscillations in a non-integrable system, it may be of great interest to analyse these photo-induced auto-oscillations. Because of the low values of the frequencies and the large amplitudes they can be experimentally investigated (for example, using magneto-optical methods) in a real time regime.

Acknowledgments

The authors are grateful to V G Bar'yakhtar, A K Kolezhuk, A S Kovalev, N E Kulagin, Yu M Fedorov and A K Zvezdin for stimulating discussions. This work was partially supported by grants of the International Science Foundation and the Science and Technology Committee of Ukraine.

References

[1] Fedorov Yu M, Leksikov A A and Aksenov A E 1983 *Pis. Zh. Eksp. Teor. Fiz.* **37** 134 (*JETP Lett.* **37** 161)
[2] Fedorov Yu M, Leksikov A A and Vorotynova O V 1985 *Solid State Commun.* **55** 1987
[3] Fedorov Yu M, Leksikov A A and Vorotynova O V 1987 *J. Magn. Magn. Mater.* **68** 383
[4] L'vov V S 1987 *Nonlinear Spin Waves* (Moscow: Nauka) (in Russian)
[5] Krupicka S 1973 *Physics of Ferrites and Related Magnetic Oxides* (Prague: Academia) (in German)
[6] Lacklison D E, Chadwik J and Page J V 1971 *J. Appl. Phys.* **42** 1445
Lackison D E, Chadwick J and Page J V 1979 *J. Phys. D: Appl. Phys.* **5** 810
[7] Seavey M H 1973 *Solid State Commun.* **12** 49
[8] Ivanov B A and Lyakhimets S N 1987 *Pis. Zh. Eksp. Teor. Fiz.* **46** 23 (*JETP Lett.* **46** 26)

[9] Zvezdin A K and Mukhin A A 1988 *Kratkie Soobshcheniya Fiz.* **5** 20 (in Russian)
[10] Bar'yakhtar V G, Ivanov B A and Chetkin M V 1985 *Usp. Fiz. Nauk* **146** 416 (*Sov. Phys.–Usp.* **28** 563)
Bar'yakhtar V G, Chetkin M V, Ivanov B A and Gadetskii S N 1994 *Dynamics of Topological Magnetic Solitons. Experiment and Theory* (*Springer Tracts in Modern Physics 129*) (Berlin: Springer)
[11] Kosevich A M and Kovalev A S 1986 *Introduction to Nonlinear Physical Mechanics* (Kiev: Naukova Dumka) (in Russian)
[12] Fedorov Yu M, Leksikov A A and Aksenov A E 1984 *Fiz. Tverd. Tela* **26** 220 (*Sov. Phys.–Solid State* **26** 128)
Fedorov Yu M, Leksikov A A and Aksenov A E 1985 *Zh. Eksp. Teor. Fiz.* **89** 2099 (*Sov. Phys.–JETP* **62** 1211)
[13] Landau L D and Lifshits E M 1958 *Mechanics* (Oxford: Pergamon)
[14] Tarasenko V V, Chenskii E V and Dikshtein I E 1976 *Zh. Eksp. Teor. Fiz.* **70** 2178 (*Sov. Phys–JETP* **43** 1128)
[15] Bar'yakhtar V G and Ivanov B A 1977 *Zh. Eksp. Teor. Fiz.* **72** 1504 (*Sov. Phys.–JETP* **45** 789)
[16] Ivanov B A, Krasnov V P and Sukstanskii A L 1978 *Fiz. Nizk. Temp.* **4** 204 (*Sov. J. Low Temp. Phys.* **4** 101)
[17] Akhiezer A I, Bar'yakhtar V G and Peletminskii S V 1968 *Spin Waves* (Amsterdam: North-Holland)
[18] Sadreev A F and Fedorov Yu M 1987 *Phys. Lett.* **123A** 148
[19] Turov E A and Shavrov V G 1984 *Usp. Fiz. Nauk* **140** 674 (1983 *Sov. Phys.–Usp* **26** 593)
[20] Ott E, Grebogi G and Yorke Y A 1990 *Phys. Rev. Lett.* **64** 1196
Shinbrot T, Grebogi G, Ott E and Yorke Y A 1993 *Nature* **363** 411
[21] Fronzoni L, Giocondo M and Pettini M 1990 *Phys. Rev.* A **43** 726
[22] Kivshar Y S, Rodelsperger F and Benner H 1994 *Phys. Rev.* E **49** 319